Energy xxx (2015) 1–13

Contents lists available at ScienceDirect

Energy

journal homepage: www.elsevier.com/locate/energy

A numerical investigation of the entropy generation in and thermodynamic optimization of a combustion chamber

H.R. Arjmandi, E. Amani*

Mechanical Engineering Dept., Amirkabir University of Technology, Tehran, Iran

ARTICLE INFO

Article history:
Received 4 August 2014
Received in revised form
10 December 2014
Accepted 17 December 2014
Available online xxx

Keywords:
EGM
Combustion chamber design
Optimization
Numerical
Exergy analysis

ABSTRACT

In this study, we are simulating the turbulent combustion of a mixed bluff-body swirl stabilized flame in a gas turbine combustion chamber and investigating the effects of different parameters, including the swirl number, distance between the air and fuel nozzle which is called bluff size, equivalence ratio, inlet fuel flow rate, and the inlet air velocity, on the entropy generation. We perform the process of the design of the combustion chamber by proposing the optimal value of each parameter based on the EGM (entropy generation minimization) method under the two maximum allowable temperature and size constraints. Two common methods of entropy generation calculation, one based on the overall entropy balance on a system and the other based on the local entropy generation rate calculation, are used and compared in this study. Our results show that the deviation between the total entropy generations calculated by the two methods is 6.4% in average which is an acceptable error in turbulent combustion simulations. Also, the two opposing factors, namely chemical reaction and heat transfer, have the main contribution to the total entropy generation.

1. Introduction

The efficient utilization of energy is a critical concern in today's design of energy systems. Scientists are trying to approach maximum efficiency in various industrial applications as much as possible. In other words, it is favorable to have minimum irreversibility. In order to achieve this goal, the exergy analysis and EGM (entropy generation minimization) method [1] can be applied to optimize the design of energy conversion systems. In this method, the design parameters of the system are changed and entropy generation is computed in each case. The optimum design corresponds to the case with the minimum entropy generation while some additional geometry and economic constraints should be satisfied. For the details of the method, one can consult the book by Bejan [1]. Bejan [2] also reported an extensive review on the applications of the EGM method in several thermal problems.

The EGM method is vastly incorporated by researchers in different applications. Li and Faghri [3] performed both the exergy balance analysis and the local entropy generation analysis to investigate the irreversibility within fuel cells. Mahian et al. [4] applied EGM to study the effect of using nanofluids on the entropy generation between two concentric rotating cylinders at constant heat flux boundary conditions. They found that the entropy generation decreases with the increase of volume fraction of nanoparticles. Makhanlall et al. [5] found an optimum optical thickness and an optimum tilt angle where the heat losses are minimized for gas filled solar collectors. Escandón et al. [6] determined the local and average entropy generation rates for the electro osmotic flow of a non-Newtonian fluid in a parallel flat plate micro channel.

EGM method has also been implemented in several heat transfer studies in pipes. For example, Ko and Ting [7] and Ko [8] reported different optimal parameters for fully developed flow in helical pipes at the constant heat flux. Jarungthammachote [9] investigated entropy generation for the pipes with different shapes of cross section, and Amani and Nobari [10,11] studied entropy generation in the entrance region of curved pipes both numerically and analytically.

EGM is extensively used for IC (internal combustion) engine problems. Caton [12] observed that, in general, availability destruction decreases when combustion temperature is increased. He [13] also examined the availability destruction in an adiabatic, constant volume combustion in a vessel. He discussed the effect of combustion temperature and equivalence ratio on the entropy

* Corresponding author. Mechanical Engineering Dept., Amirkabir University of Technology, 424 Hafez Avenue, Tehran, P.O.Box: 15875-4413, Iran. Tel.: +98 21 64543404.

E-mail addresses: h.r.arjmandi@aut.ac.ir (H.R. Arjmandi), eamani@aut.ac.ir (E. Amani).

http://dx.doi.org/10.1016/j.energy.2014.12.077
0360-5442/

Nomenclature

Latin symbols

A	area
C_p	specific heat
D	mass diffusion coefficient
E	energy
G_k	production of turbulent kinetic energy
h	enthalpy
J_i	diffusion flux of ith species
k	turbulent kinetic energy
M_i	molecular weight of ith species
P	pressure
Q	volume flow rate
$\overline{R}$	universal gas constant
R_i	mass rate of creation of ith species by chemical reaction
r	radial coordinate
S	swirl number, modulus of mean rate of strain, global entropy generation rate
S_{ij}	mean strain rate
Sc	Schmidt number
S'''	local entropy generation rate
s	specific entropy
T	temperature
u	velocity
V_a	mean air-inlet velocity
Y_i	mass fraction of ith species
Z	mixture fraction
z_i	mass fraction of ith atomic species
x	axial coordinate
X_i	mole fraction of ith species

Greek symbols

α	inverse effective Prandtl number
ξ	bluff-size ratio
ε	turbulent energy dissipation rate
Φ	equivalence ratio
λ	thermal conductivity
μ	dynamic viscosity
μ_i	chemical potential of ith species
ρ	density
τ	stress tensor

Subscripts

a	air
b	bluff body
ch	due to chemical reaction
eff	effective
f	fuel
gen	entropy generation due to all phenomena
h	due to heat transfer
i,j	species index, coordinate index
m	due to mass transfer
n	normal component
t	turbulent
v	due to viscous dissipation

generation. Rakopoulos and Kyritsis [14] Compared the entropy generation of the internal combustion engine operation for methane, methanol, and dodecane fuels. Nakonieczny [15] investigated entropy generation in the charge exchange system of a turbocharged, intercooled diesel engine and discussed the effect of various variables, such as the intercooler air temperature, air pipe length, and timings of inlet valve closure and exhaust valve opening, on the entropy production. Rakopoulos and Kyritsis [16] studied entropy generation during the combustion of the hydrogen-enriched natural and landfill gas. Finally, Rakopoulos and Giakoumis [17] presented comprehensive reviews of the studies on the availability analyses of IC engines published up to 2006. They reported fruitful conclusions about the availability destruction, heat transfer rates, and availability expelled with the exhaust gas. Also, they concluded that less availability is destroyed with lighter fuels such as methane and methanol compared to the longer-chain hydrocarbons which is attributed to the lower entropy generation of the decomposition of lighter molecules. Sieniutycz [18] investigated the relationship between entropy generation and some parameters, like fuel consumption and power generation, in an engine. The availability analysis of a spark ignition biogas–hydrogen engine during the closed part of the engine cycle was performed by Rakopoulos and Michos [19]. Knizley et al. [20] investigated the effects of the fuel type, reactant temperature, reactant pressure, fuel-air equivalence ratio and diluents on the entropy generation and availability destruction in a constant energy-volume (UV) combustion process.

In addition to IC engines, exergy analysis and EGM has been applied to other single- and multi-phase combustion processes. Dash and Som [21] investigated the transport processes and associated irreversibility of droplet combustion in a convective medium. In a later study, Dash and Som [22] analyzed thermodynamic irreversibility of the spray combustion process for different inlet pressures, temperatures, and swirls. Datta [23] studied the entropy generation of a confined laminar diffusion flame and the influences of the inlet air temperature, heat loss through the wall, and equivalence ratio on the total rate of entropy generation. Also, Nishida et al. [24] investigated the effects of these parameters on the entropy generation of both premixed and diffusion flames. Datta [25] extended his previous study [23] to account for the role of gravity on the entropy generation. He concluded that the entropy generation increases by decreasing gravity. Stanciu et al. [26] investigated the irreversibility in both laminar and turbulent diffusion flames. Two combustion models are used by them; the multi-species approach based on the eddy-break-up model for the mean reaction rate, and the assumed probability density function for a conserved scalar that relies on the flame sheet model. Yapici et al. [27–29] investigated the effects of oxygen fraction in the air, equivalence ratio, and swirl on the entropy generation in methane- and hydrogen-fueled combustion chambers. They also compared the local entropy generation for different fuels [30]. Entropy generation during burning of a spherical fuel droplet was calculated by Raghavan et al. [31]. Investigation of the influence of swirl angle on the irreversibility in a turbulent diffusion flame was performed by Stanciu et al. [32]. Som and Datta [33] performed a fundamental study on the thermodynamic irreversibility in the processes of combustion of gaseous, liquid, and solid fuels. They discussed the effects of the free stream velocity, particle diameter, ambient temperature, and gravity on the entropy generation rate in both upward and downward flows. They reported the decrease of the entropy generation by reducing the Froude number. Analysis of the entropy generation of laminar propagating hydrogen-enriched co-flow methane-air triple flames was conducted by Briones et al. [34]. Chen [35] investigated the entropy generation of laminar premixed

Please cite this article in press as: Arjmandi HR, Amani E, A numerical investigation of the entropy generation in and thermodynamic optimization of a combustion chamber, Energy (2015), http://dx.doi.org/10.1016/j.energy.2014.12.077

hydrogen-air combustion of planar opposing jets. Chen et al. [36] investigated the effects of hydrogen addition to methane on the entropy generation in a similar flame. The effect of equivalence ratio and hydrogen addition to methane-air laminar counter-flow diffusion flames were also investigated by Chen et al. [37,38]. Bidi et al. [39] studied the entropy generation of combustion in porous media. Sheikhi et al. [40,41] analyzed local entropy generation of turbulent flows using LES (large eddy simulation). Emadi and Emami [42] evaluated entropy generation rate and exergy loss in a turbulent non-premixed hydrogen-enriched bluff-body flame. Makhanlall et al. [43] performed the second law analysis of turbulent diffusion natural gas flames and investigated the importance of radiative energy devaluation. Entropy generation in turbulent premixed flames was analyzed by Farran and Chakraborty [44] based on a simple chemistry Direct Numerical Simulation database with a range of different values of heat release parameter and global Lewis number, spanning both the corrugated flamelet and thin reaction zone regimes of combustion. In addition, numerical simulation of biogas flameless combustion was performed by Hosseini et al. [45] to analyze the entropy generation and emission in this regime. A numerical model was developed for the entropy generation and exergy destruction analysis of hydrogen/air premixed flames in micro-combustors with baffles for different baffles height and mass flow rates by Jiang et al. [46]. Rana et al. [47] evaluated the exergy transfer and its destruction due to thermodynamic irreversibility in the process of flame stabilization in a heat recirculating micro combustor.

In the present study, we are investigating the effects of different design parameters on the entropy generation of methane-air combustion in a gas turbine combustion chamber. This involves the study of two important geometrical parameters, i.e. the area of the air-inlet nozzle and the distance between the air and fuel nozzle called bluff size, which affect the fuel-air mixing process. In addition, the impact of the inlet air swirl is investigated. Experiments show that these parameters have considerable influence on the mixing and pollutant formation. We also investigate the effect of equivalence ratio and its interaction with the other parameters on the entropy generation rate. The optimal design is proposed based on the EGM method and we discuss how different parameters affect the maximum temperature and flame height. Two common methods of entropy generation calculation, one based on applying the entropy balance on the system and the other based on the local entropy generation rate calculation, are used and compared in this study. Here, we call the first method the direct method because it is based on direct implementation of the second law of thermodynamics on a system. The second method which is used mostly in CFD (computational fluid dynamics) studies is called the indirect method here. This method makes it possible to study the entropy generation due to each phenomenon present in a problem. Yapici et al. [28] performed a study to obtain the optimum equivalence ratio and swirl number, but he only considered the entropy generation due to the viscous friction and heat transfer, while we consider the entropy generation due to chemical reaction, mass transfer, and coupling between mass and heat transfer processes in addition to those factors considered by Yapici et al. [28]. We show that not only are these entropy generation rates important in combustion problems, but also they can have dominant contribution to the total entropy generation rate and cannot be neglected.

2. Mathematical model

2.1. Governing equations

In this study, we use RNG (renormalization group) k-ε model for the turbulence closure and the eddy-dissipation model for the combustion. The choice of these models is based on the trade-off between accuracy and computational cost in our study which requires the simulation of a large number of combustion chamber topologies and operating conditions. Although, the large eddy simulation offers a more accurate turbulence closure, its usage is limited due to the high computational costs. Hence, the RANS (Reynolds-averaged Navier–Stokes) based closures have still the main roll in practical engineering combustion chamber simulation and design [48]. For the problem of our interest, the RNG k-ε model with the modifications accounting for the swirl is a wise compromise between the accuracy and computational cost. Here, the two-step Westbrook–Drier reaction mechanism [49] which is appropriate for fuel lean mixtures governs the chemistry.

In the following paragraphs, the governing equations used in our study are introduced. All equations are given using Cartesien coordinate notation where the summation convention over repeated indices is implied. The governing equations are the transport of chemical species as

$$\frac{\partial}{\partial x_j}\left(\rho u_j Y_i\right) = -\frac{\partial}{\partial x_j} J_{i,j} + R_i \tag{1}$$

where u_j is the jth component of the (mean) velocity vector, ρ is the density of the mixture, Y_i is the local mass fraction of species i, R_i is the mass rate of creation or depletion of species i by the chemical reaction, and J_i is the total, molecular and turbulent, flux of species i and is modeled by

$$J_{i,j} = -\rho D_{eff} \frac{\partial Y_i}{\partial x_j} \tag{2}$$

where D_{eff} is the effective mass diffusivity of each species in the mixture and defined in the RNG model as

$$D_{eff} = \frac{\rho \alpha}{\mu_{eff}} \tag{3}$$

and α is computed by the following equation

$$\left|\frac{\alpha - 1.3929}{\alpha_0 - 1.3929}\right|^{0.6321} \left|\frac{\alpha + 2.3929}{\alpha_0 + 2.3929}\right|^{0.3679} = \frac{\mu}{\mu_{eff}} \tag{4}$$

where $\alpha_0 = 1/Sc$ and Sc is the molecular Schmidt number defined by

$$Sc = \frac{\mu}{\rho D} \tag{5}$$

and D, ρ, μ, and μ_{eff} are the molecular mass diffusivity, density, molecular viscosity, and effective viscosity of the mixture, respectively.

The momentum equation is written by

$$\frac{\partial}{\partial x_j}\left(\rho u_i u_j\right) = -\frac{\partial P}{\partial x_i} + \frac{\partial \tau_{ij}}{\partial x_j} \tag{6}$$

where P is the pressure and τ_{ij} is the effective stress tensor.

$$\tau_{ij} = \mu_{eff}\left(\frac{\partial u_i}{\partial x_j} + \frac{\partial u_j}{\partial x_i}\right) - \frac{2}{3}\mu_{eff}\frac{\partial u_l}{\partial x_l}\delta_{ij} \tag{7}$$

The energy conservation equation is

$$\frac{\partial}{\partial x_j}\left[u_j(\rho E + P)\right] = \frac{\partial}{\partial x_j}\left(\lambda_{eff}\frac{\partial T}{\partial x_j} - \sum_i h_i J_{i,j} + u_j \tau_{ij}\right) + S_h \tag{8}$$

where $S_h = -\sum_i h^0_{f,i} R_i$ includes the heat of chemical reaction,

Please cite this article in press as: Arjmandi HR, Amani E, A numerical investigation of the entropy generation in and thermodynamic optimization of a combustion chamber, Energy (2015), http://dx.doi.org/10.1016/j.energy.2014.12.077

$$E = h - \frac{P}{\rho} + \frac{u_j u_j}{2} \tag{9}$$

h is the sensible enthalpy, and $h^0_{f,i}$ the formation enthalpy of species i. λ_{eff} is the effective conductivity and is given by

$$\lambda_{eff} = \alpha C_p \mu_{eff} \tag{10}$$

where α in Eq. (10) is computed from Eq. (4) substituting $\alpha_0 = \lambda/\mu C_p$. λ is the molecular conductivity and C_p is the mixture specific heat capacity.

Two additional equations in RNG k–ε turbulence model are

$$\frac{\partial}{\partial x_j}(\rho u_j k) = \frac{\partial}{\partial x_j}\left(\alpha_k \mu_{eff}\frac{\partial k}{\partial x_j}\right) + G_k - \rho\varepsilon \tag{11}$$

$$\frac{\partial}{\partial x_j}(\rho u_j \varepsilon) = \frac{\partial}{\partial x_j}\left(\alpha_\varepsilon \mu_{eff}\frac{\partial \varepsilon}{\partial x_j}\right) + \frac{\varepsilon}{k}(C_{1\varepsilon}G_k - C_{2\varepsilon}\rho\varepsilon) - \chi \tag{12}$$

where k is the turbulence kinetic energy and ε is its dissipation rate. α_k and α_ε are the inverse effective Prandtl numbers for k and ε, respectively, and are calculated from Eq. (4) substituting $\alpha_0 = 1$. The effective viscosity in RNG k–ε turbulence model is computed by

$$\mu_{eff} = \mu + \mu_t, \quad \mu_t = \rho C_\mu \frac{k^2}{\varepsilon} \tag{13}$$

and

$$G_k = \mu_t S^2 \tag{14}$$

$$\chi = C_\mu \rho \frac{\eta^3\left(1 - \frac{\eta}{\eta_0}\right)}{1 + \beta\eta^3}\frac{\varepsilon}{k} \tag{15}$$

$$\eta = S\frac{k}{\varepsilon} \tag{16}$$

where S_{ij} is the mean rate of strain tensor and defined as

$$S_{ij} = \frac{1}{2}\left(\frac{\partial u_i}{\partial x_j} + \frac{\partial u_j}{\partial x_i}\right) \tag{17}$$

and its modulus, S, is given by

$$S = \sqrt{2 S_{ij} S_{ij}} \tag{18}$$

The constants of the model are $C_\mu = 0.0845$, $C_{1\varepsilon} = 1.42$, $C_{2\varepsilon} = 1.68$, $\eta_0 = 4.38$ and $\beta = 0.012$.

The mixture density is calculated using the ideal gas law. Combining the properties of different species, the properties of the mixture are calculated; for the mixture specific heat, the linear rule, i.e. $C_p = \sum_i Y_i C_{p,i}$, is used where $C_{p,i}$'s, as well as s^0_i's in Eq. (20), of different species are determined as a function of temperature from the 7-coefficent NASA polynomials [50]; and for the transport coefficients of the mixture, including molecular viscosity, diffusivity, and conductivity, the "Wilke rule" [51] is used where the molecular transport properties of each species are assumed constant and given in Table 1. Note that the constant molecular transport properties assumption has a negligible effect on the results since these properties are about two, or even more, orders of magnitude smaller than their turbulent counterparts. The sensible enthalpy is related to the mixture specific heat via $h = \int_{T_{ref}}^{T} C_p dT$.

Table 1
The molecular properties of species used in our study. $D_i = 2.88 \times 10^{-5} m^2/s$ for all species.

Species	μ_i (kg/ms)	λ_i (w/m K)
CH_4	0.0332	1.087×10^{-5}
O_2	0.0246	1.919×10^{-5}
CO_2	0.0145	1.370×10^{-5}
CO	0.0250	1.750×10^{-5}
H_2O	0.0261	1.340×10^{-5}
N_2	0.0242	1.663×10^{-5}

2.2. Entropy generation calculation

Here, we calculate the entropy generation using two approaches. In the first method, which is called "direct method" hereafter, we use the second law directly to compute the total entropy generation rate in a system, i.e. for an adiabatic combustion chamber performing no work on its surrounding; the total rate of entropy generation equals the net outflow of entropy from the system

$$S_{gen} = S_{out} - S_{in} \cong \oint_{A_{out}} \rho\left(\sum_i Y_i s_i\right) u_n dA - A_{in}\oint_{A_{in}} \rho\left(\sum_i Y_i s_i\right) u_n dA \tag{19}$$

Therefore, S_{gen} is computed by integrating mass flux of entropy over the inlet and outlet boundaries. Note that, s_i is the entropy of species i in the mixture, i.e.

$$s_i = s_i(T, P_i) = s^0_i(T) - \frac{\overline{R}}{M_i} ln\left(\frac{X_i P}{P_0}\right) \tag{20}$$

where $\overline{R}$ is the universal gas constant.

In the second method, called "indirect method", we calculate the local entropy generation rates (per unit volume) due to different phenomena present in our problem. The causes of entropy generation in a single-phase combustion problem are the viscous friction, heat transfer, mass diffusion, coupling term between the mass and heat transfer, and chemical reaction [52]. These rates can be written as

$$S'''_v = \frac{\tau_{ij}}{T}\left(\frac{\partial u_i}{\partial x_j}\right) \tag{21a}$$

$$S'''_h = \frac{\lambda_{eff}}{T^2}\left(\frac{\partial T}{\partial x_j}\frac{\partial T}{\partial x_j}\right) \tag{21b}$$

$$S'''_m = \sum_i \frac{\rho \overline{R} D_{eff}}{Y_i M_i}\left(\frac{\partial Y_i}{\partial x_j}\frac{\partial Y_i}{\partial x_j}\right) \tag{21c}$$

$$S'''_{coupling} = \sum_i \frac{\rho s_i D_{eff}}{T}\left(\frac{\partial Y_i}{\partial x_j}\frac{\partial T}{\partial x_j}\right) \tag{21d}$$

$$S'''_{ch} = -\sum_i \frac{\mu_i \omega_i}{T} \tag{21e}$$

where μ_i is the chemical potential of species i in the mixture which is given by

Please cite this article in press as: Arjmandi HR, Amani E, A numerical investigation of the entropy generation in and thermodynamic optimization of a combustion chamber, Energy (2015), http://dx.doi.org/10.1016/j.energy.2014.12.077

$$\mu_i = h^0_{f,i} + h_i - Ts_i \tag{22}$$

The rates in Eq. (21a–e) are also given in axisymmetric coordinates in Appendix A. The total entropy generation rate per unit volume, S'''_{gen}, is the sum of all local rates in Eq. (21). Eventually, the total entropy generation rate in the system is obtained by integrating S'''_{gen} over the entire system.

$$S_{gen} = \oint_V S'''_{gen} dV \tag{23}$$

3. Numerical method

The geometry of the combustion chamber and a typical grid used in this study are shown in Fig. 1. r_0 is the radius of the combustion chamber, r_1 the outer radius of the air-inlet nozzle, r_2 the inner radius of this nozzle, and r_3 the radius of the fuel inlet nozzle.

For the numerical discretization of the governing equations, finite volume method is applied. The diffusion terms are discretized by the second-order central scheme and convection terms by the standard second-order upwind scheme [53]. The SIMPLE algorithm [54] is used for the pressure–velocity decoupling of the Navier–Stokes equations. The standard non-linear limiter, which is derived from the work of Barth and Jespersen [55], is incorporated to preserve the monotonicity of the convection discretization scheme.

3.1. Verification and validation

To report the grid sensitivity test, the profile of different parameters in various cross sections of the chamber are depicted in Figs. 2–4. In these figures, one case corresponds to the typical grid shown in Fig. 1 and the other case corresponds to a refined grid obtained by dividing each computational cell of the typical grid to four cells. It is observed that the results of different grids are in fine agreement with each other and, therefore, the grid independency of the solution is confirmed.

In order to check our entropy generation calculations, we also verify our numerical computation for a special case, i.e. the laminar flow in a straight duct with constant heat flux at the wall which has an analytical solution for the profiles of the entropy generation rate due to the viscous friction and heat transfer at the fully developed cross section. In this case, no estimation is required to compute the entropy generation in contrast to the turbulent flame cases reported in our study. Therefore, the only source of error is numerical errors which can be evaluated through this verification. The comparison is illustrated in Fig. 5 for water flow in a duct with radius $r_0 = 6$ mm, $u_0 = 0.01$ m/s, $T_0 = 273$ K, and $q'' = 1000\text{W/m}^2$. The analytical solutions for the entropy generation rate profiles are

$$S'''_h = \frac{q''^2}{\lambda T^2}\left\{\left[\frac{2\alpha}{u_m r_0}\right]^2 + \left[2\left(\frac{r}{r_0}\right) - \left(\frac{r}{r_0}\right)^3\right]^2\right\} \tag{24}$$

$$S'''_v = \frac{16\mu}{T}\left(\frac{u_m}{r_0}\right)^2\left(\frac{r}{r_0}\right)^2 \tag{25}$$

where $\alpha = \lambda/\rho c_p$ and T_m and u_m are the bulk temperature and velocity of the flow in each cross section. As it can be observed in these figures, our calculations are in close agreement with the analytical solutions.

Subsequently, in order to validate the present model, we simulate the well-known methane-air turbulent non-premixed jet flame "Sandia flame D" and compare the results of our model with the experimental measurements [56]. This flame has also been used for entropy generation validation by Sheikhi et al. [40]. For the details of the burner geometry and inlet boundary profiles, readers can refer to the corresponding web page [56]. We use the same boundary conditions and computational grid as our previous study [57] while the present model differs. The mean entropy is extracted from the measured instantaneous temperature and species mass fractions [40,56]. As it is observed in Fig. 6, the computed results have in average 9.5% overprediction with respect to the experiment which is within the acceptable range of the errors of estimations described in the following section. This deviation in entropy prediction is mainly due to temperature overprediction, typical of RANS/Eddy-dissipation models [57]. Note also that neglecting the radiation effect generally results in an overprediction of the flame temperature, but for such a non-sooty methane-air flame, i.e. Sandia D, this simplification does not lead to significant errors (about 8% overprediction as investigated by Xu et al. [58]).

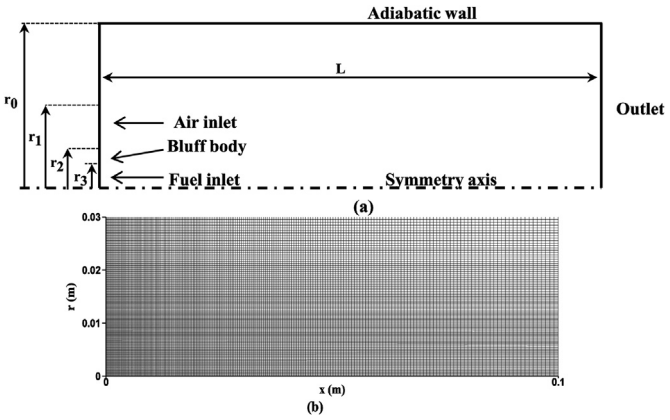

Fig. 1. a) The geometry of combustion chamber and b) a part of combustion chamber near the inlet and the typical (146 × 400) grid used for the simulations.

4. Results and discussion

4.1. Case studies

The bluff size, or the width of the wall between the air and fuel nozzle, has an important effect on the mixing and efficiency of the combustion in a gas turbine combustion chamber. To study the effect of the bluff size, we define a new dimensionless parameter as

$$\xi = \frac{A_a}{A_b} \tag{26}$$

where A_a is the area of the air-inlet nozzle and A_b is the area of the annular wall (bluff) between the air-inlet and fuel-inlet nozzles. Hereafter, ξ is called bluff-size ratio. Simulations are carried out for the bluff-size ratio in the range 0.5–10. The other important factor is the air-inlet swirl. The well-known swirl number parameter, S, which is the ratio of tangential to axial momenta

$$S = \frac{\int_{r_2}^{r_1} u_x u_\theta r^2 dr}{r_1 \int_{r_2}^{r_1} u_x^2 r dr} \tag{27}$$

is used to quantify the swirl intensity. Here, we study the effect of swirl number in the range 0–0.4. The 3rd design parameter is the air-inlet velocity, V_a, which can be changed by altering the air-inlet

Please cite this article in press as: Arjmandi HR, Amani E, A numerical investigation of the entropy generation in and thermodynamic optimization of a combustion chamber, Energy (2015), http://dx.doi.org/10.1016/j.energy.2014.12.077

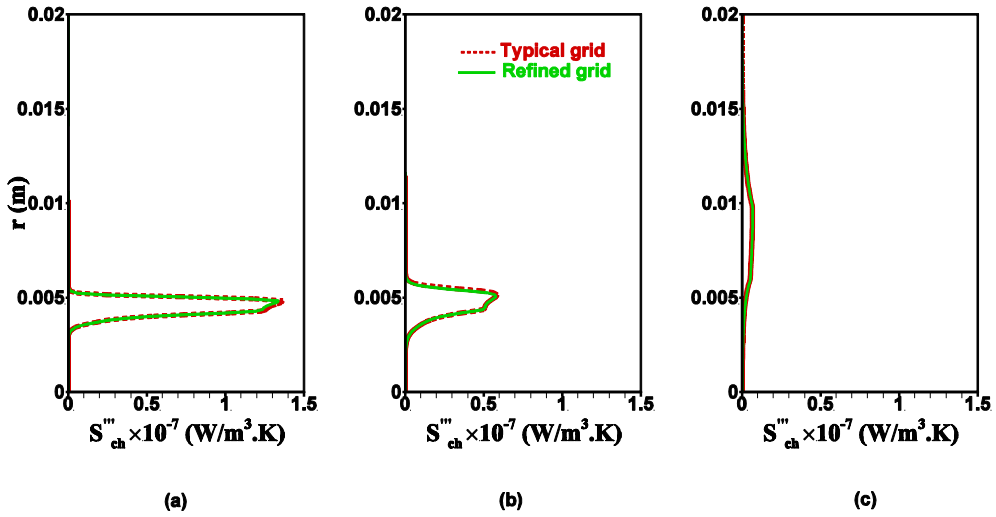

Fig. 2. The profiles of the local entropy generation rate due to chemical reaction at different cross sections using the typical grid (146 × 700) and the refined grid (292 × 800) a) x = 0.4 cm, b) x = 1 cm, and c) x = 10 cm.

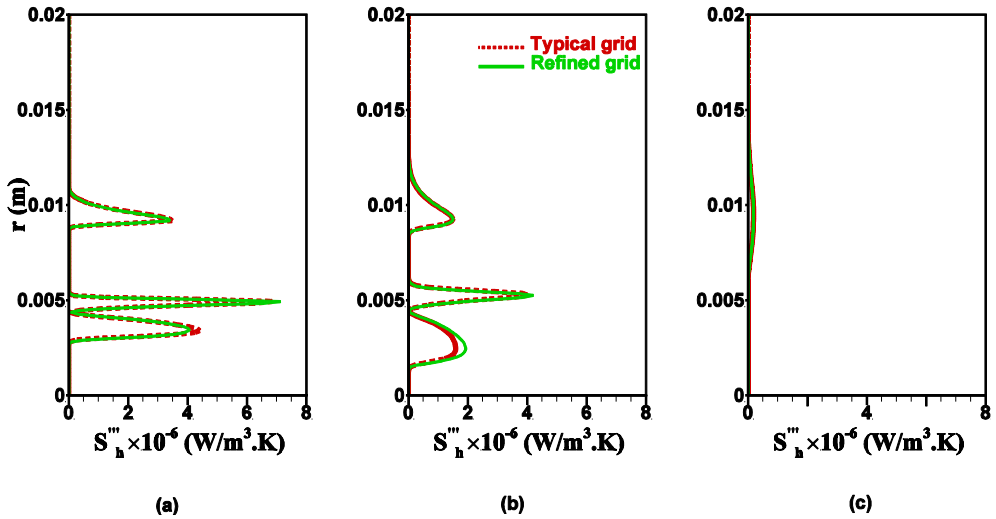

Fig. 3. The profiles of the local entropy generation rate due to heat transfer at different cross sections using the typical grid (146 × 700) and the refined grid (292 × 800) a) x = 0.4 cm, b) x = 1 cm, and c) x = 10 cm.

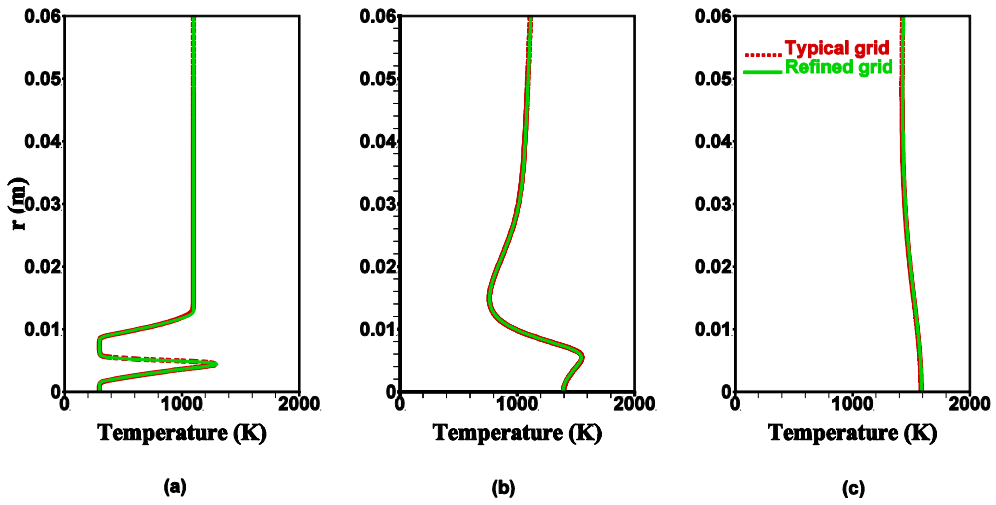

Fig. 4. The profiles of the temperature at different cross sections using the typical grid (146 × 700) and the refined grid (292 × 800) a) x = 0.4 cm, b) x = 1 cm, and c) x = 10 cm.

Please cite this article in press as: Arjmandi HR, Amani E, A numerical investigation of the entropy generation in and thermodynamic optimization of a combustion chamber, Energy (2015), http://dx.doi.org/10.1016/j.energy.2014.12.077

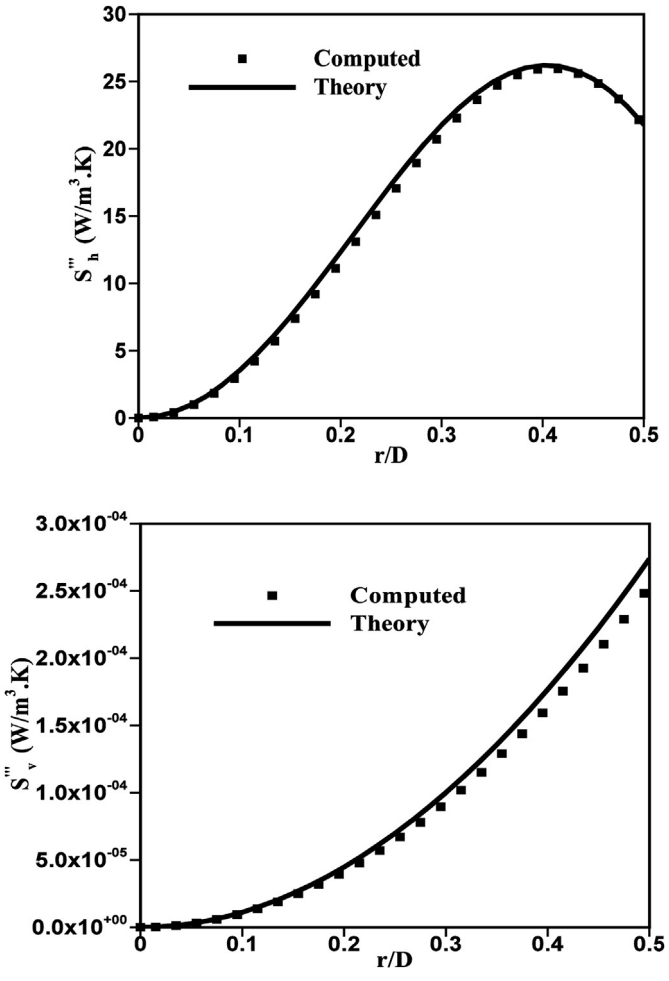

Fig. 5. The local entropy generation rate at section x/D = 65; up: due to heat transfer, down: due to viscous friction.

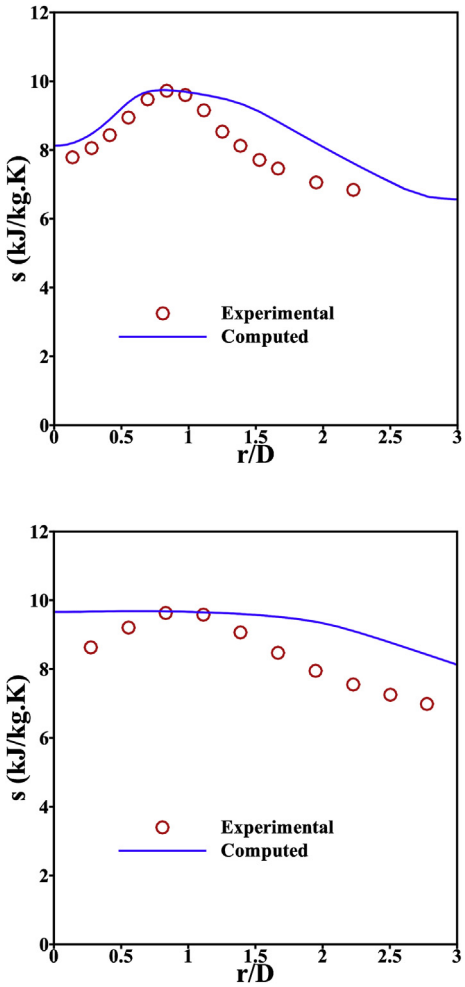

Fig. 6. Comparison of the present model prediction and experimental data (Ref. [56]). The radial profile of the mixture specific entropy, $s = \sum_i Y_i s_i$, at two cross sections; x/D = 7.5 (up) and x/D = 15 (down). D = 7.2 *mm* is the fuel nozzle diameter. Note that to determine the total entropy generation rate between the inlet and a specific cross section, this profile is integrated using Eq. (19) over that cross section, e.g. A_{out}: x/D = 7.5 or A_{out}: x/D = 15.

nozzle area assuming constant air flow rate. We consider different values of the air-inlet velocity in the range 3.969–31.752 m/s in our simulations. The other important design parameter is the equivalence ratio, ϕ, which indicates the ratio of air to fuel mass flow rates. This parameter takes different values in the range 0.5–1.4 in our simulations. We also consider different working condition of the combustion chamber by taking into account the different values of fuel-inlet flow rate in the range 5–10 lpm (liter per minute). Other geometrical parameters of the combustion chamber (see Fig. 1) are $r_0 = 6$ cm, $r_3 = 0.4$ cm, $L = 50$ cm. Note that, r_1 and r_2 take different values in the range 0.714–1.721 cm and 0.438–1.197 cm, respectively, for introducing different ξ or V_a.

4.2. Entropy generation minimization

As it was mentioned earlier, using indirect method enables us to study the effect of different phenomena on the entropy generation separately. Beside this fact, using these two methods for the total entropy generation calculation and comparing them has another advantage. To explain this advantage, note that the formulae of both direct method, Eq. (19), and indirect method, Eq. (21), include the multiplication of different variables, i.e. non-linear terms. Using these formulae for turbulent flows replacing the instantaneous variables with their means and molecular transport coefficients, μ, λ, and D, with the effective transport coefficients, μ_{eff}, λ_{eff}, and D_{eff}, is an approximation. Therefore, computing and comparing the total entropy generation using these two independent approximations would be extremely useful to validate conclusions extracted from our results. Note also that using such approximations for calculating the entropy generation in turbulent flows is unavoidable. This is because the instantaneous formulation, see Eq. (21), involves the gradient of different variables. Therefore, the exact calculation of the entropy generation requires the usage of two-point PDF (probability density function) methods which include the gradients of all variables, in addition to the variables themselves, as the state variables and is beyond the current scope of turbulent combustion modeling and simulation.

Fig. 7 shows the total entropy generation calculated using both direct and indirect methods for quite a lot of simulation cases involving different equivalence ratios and inlet-fuel flow rates. The results of both methods are in satisfactory agreement especially where $\phi < 0.7$. The maximum deviation between the two methods reaches about 16% at the fuel-lean limit. The deviation between the two methods is depicted in Fig. 8. The average deviation for all simulations is 6.4% which is acceptable in turbulent combustion modeling and supports the assumptions underlying the entropy generation calculations in our study. As it is observed in Fig. 7, the total entropy generation reduces by increasing the equivalence

Please cite this article in press as: Arjmandi HR, Amani E, A numerical investigation of the entropy generation in and thermodynamic optimization of a combustion chamber, Energy (2015), http://dx.doi.org/10.1016/j.energy.2014.12.077

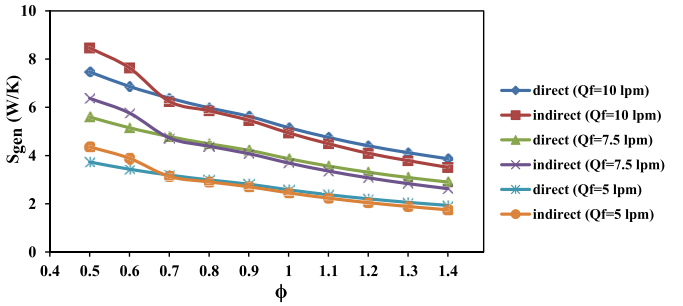

Fig. 7. The entropy generation rates for various equivalence ratios and inlet-fuel flow rates. Note that lpm in the figures refers to liter per minute. The other parameters are $S = 0$, $A_a = 2$ cm^2, $\xi = 10$, and $T_{inlet} = 298.15$ K.

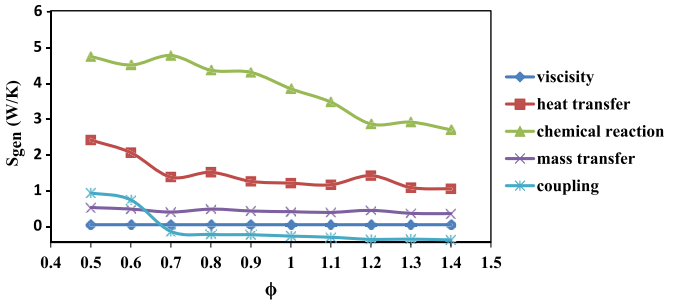

Fig. 9. The entropy generation rate due to different phenomena versus equivalence ratio. The other parameters are $Q_f = 10$ lpm, $S = 0$, $A_a = 2$ cm^2, $\xi = 10$, and $T_{inlet} = 298.15$ K.

ratio and an optimum case cannot be proposed based on EGM. This trend was also reported by Yapici et al. [28] in spite of the fact that they only considered viscous and heat transfer entropy generation rates. This behavior can be explained via Fig. 9. This figure shows that the entropy generations due to chemical reaction and heat transfer have the dominant contributions to the total entropy generation in the combustion chamber. This conclusion is also confirmed by the next results and diagrams presented in this paper. According to Fig. 9, increasing the equivalence ratio towards the fuel-rich region causes the heat transfer and especially chemical entropy generations, i.e. the dominant parts of the total entropy generation, to decrease monotonically. This is due to the drop of combustion intensity and the resulted heat release by enriching the fuel in the combustion chamber.

Therefore, the optimal value of the equivalence ratio cannot be chosen only based on minimizing the entropy generation and is usually selected based on the combustion efficiency and the MAT (maximum allowable temperature) in the combustion chamber. However, the MAT criterion and other criteria, e.g. geometrical, economical, etc., can be regarded as the constraints in the EGM method which results in an optimization problem under several constraints. Note that, the equivalence ratio is the most effective parameter of controlling the maximum temperature in the combustion chamber. This can also be seen in our results by comparing Fig. 10 and the results of the next parts. The MAT criterion is important from two different aspects; one corresponds to the thermal resistance of materials used to fabricate the combustion chamber and other downstream parts, e.g. turbine blades. The other concern is related to the pollutant emission control because this temperature is the prominent factor affecting the NOX (mono-nitrogen oxides) production. To account for the MAT constraint, the maximum temperature within the combustion chamber is also reported in Fig. 10. For example, if MAT equals 1900 *K*, the value of equivalence ratio is limited to $\phi = 0.5$. This choice also corresponds to a fuel-lean condition typical of practical combustion chambers. Beside MAT constraint, we consider another constraint regarding the size of the combustion chamber which is discussed separately in section 4.3. We also checked all of our optimizations presented in this part to satisfy this second constraint. Therefore, our optimizations are actually performed under two constraints.

In the next step, we investigate the effect of the bluff-size on the entropy generation and try to propose a superior design based on EGM method. The total entropy generation within the combustion chamber is reported for different bluff-size ratios in Fig. 11 using both direct and indirect methods. The maximum temperature within the combustion chamber is also shown in this figure to perform an optimization under the MAT constraint. The deviation between the direct and indirect methods is about 13% which is acceptable. Note that the average deviation is far below this value because for this case; $\phi = 0.5$ which is in fuel-lean region (refer to Fig. 8). Another interesting point which is inferred from Fig. 11 is that in spite of some deviation between the total entropy generations computed by the two methods, the optimum condition proposed by both of them is approximately identical. In other words, both methods result in the same optimal design. This further supports the optimal conditions proposed in our study. As it can be observed in Fig. 11, the optimum condition, corresponding to the

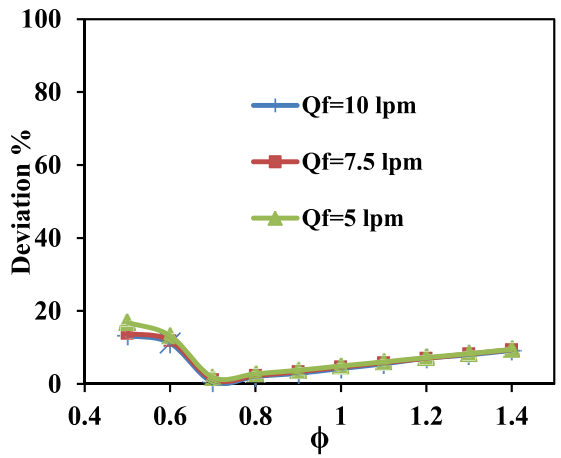

Fig. 8. The deviation between direct and indirect methods of entropy generation calculation.

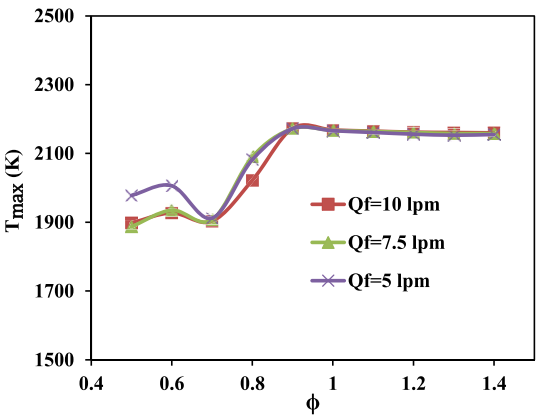

Fig. 10. The maximum temperature within the combustion chamber for various equivalence ratios and inlet-fuel flow rates. The other parameters are $S = 0$, $A_a = 2$ cm^2, $\xi = 10$, and $T_{inlet} = 298.15$ K.

Please cite this article in press as: Arjmandi HR, Amani E, A numerical investigation of the entropy generation in and thermodynamic optimization of a combustion chamber, Energy (2015), http://dx.doi.org/10.1016/j.energy.2014.12.077

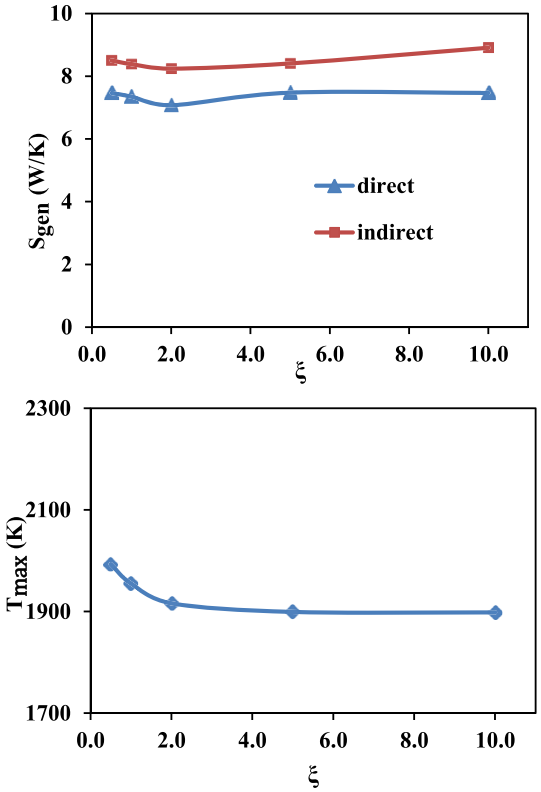

Fig. 11. The total entropy generation versus the bluff-size ratio computed using direct and indirect methods (up), and maximum temperature inside the combustion chamber versus the bluff-size ratio (down). The other parameters are $Q_f = 10$ lpm, $S = 0$, $A_a = 2$ cm^2, $\phi = 0.5$, $V_a = 15.876$ m/s, and $T_{inlet} = 298.15$ K.

minimum total entropy generation under the constraint of $MAT \approx 1900K$, is at $\xi = 2$. The next figures explain this result further. Fig. 12 shows the entropy generation rate due to different phenomena separately. According to this figure, the entropy generation due to chemical reaction increases by the increase of the bluff-size ratio while the heat transfer entropy generation decreases. These two phenomena make the main contribution to the total entropy generation. This behavior is explained through Figs.13–15. For three values of the bluff-size ratio, the flow streamlines are depicted in Fig. 13, and the contours of the fuel mass fraction and temperature are depicted in Figs. 14 and15, respectively. Note that these figures show a part of the combustion chamber near the inlets. For example, in Fig. 13, one can see the eddies generated in the central recirculating region of the chamber near the inlet streams. There is also another eddy which generated near the corner of the combustion chamber due to the flow expansion and is out of the depicted frame in Figs. 13–15. This region is called the corner recirculating region in a combustion chamber. For the sake of completeness, this corner region is shown in Fig. 16 where you can see the corner eddy. The eddies in central recirculating region play an important role in fuel-air mixing. As it is observed in Fig. 13, by decreasing the bluff-size ratio, i.e. increasing the bluff area with respect to the air-inlet area, the number and complexity of the generated eddies increases. This leads to the increase in the mixing rate which reduces the chemical entropy generation rate while the entropy generation rate due to heat transfer rises due to the increase in the reaction heat release (see Fig. 12). In other words, the chemical entropy and heat transfer entropy are opposing phenomena in the optimization of the bluff-size ratio. The trade-off between these opposing rates occurs at $\xi = 2$ corresponding to the minimum total entropy generation. Considering the maximum temperature versus the bluff-size ratio in Fig. 11, this optimum condition also satisfies the MAT constraint.

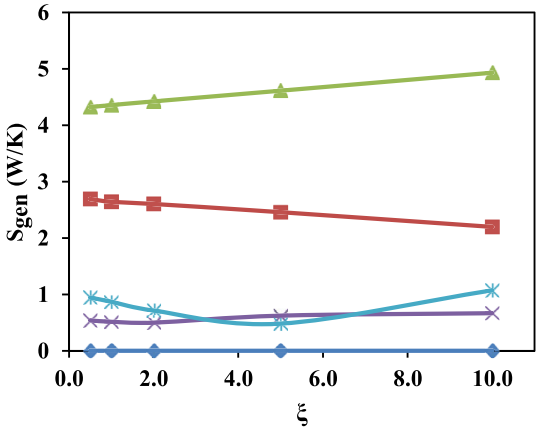

Fig. 12. The entropy generation rate due to different phenomena versus the bluff-size ratio. The other parameters are $Q_f = 10$ lpm, $S = 0$, $A_a = 2$ cm^2, $\phi = 0.5$, $V_a = 15.876$ m/s, and $T_{inlet} = 298.15$ K. Line legend: the same as Fig. 9.

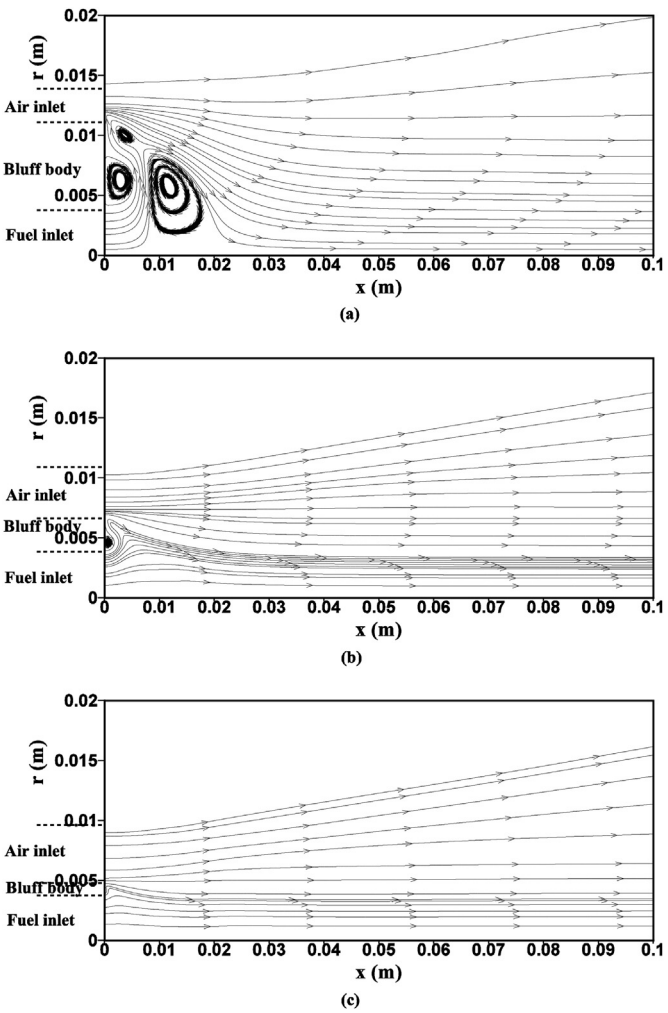

Fig. 13. Streamlines in a part of the combustion chamber, near the inlets, for a) $\xi = 0.5$, b) $\xi = 2$ (optimized case), and c) $\xi = 10$. The other parameters are $Q_f = 10$ lpm, $S = 0$, $A_a = 2$ cm^2, $\phi = 0.5$, $V_a = 15.876$ m/s, and $T_{inlet} = 298.15$ K.

Please cite this article in press as: Arjmandi HR, Amani E, A numerical investigation of the entropy generation in and thermodynamic optimization of a combustion chamber, Energy (2015), http://dx.doi.org/10.1016/j.energy.2014.12.077

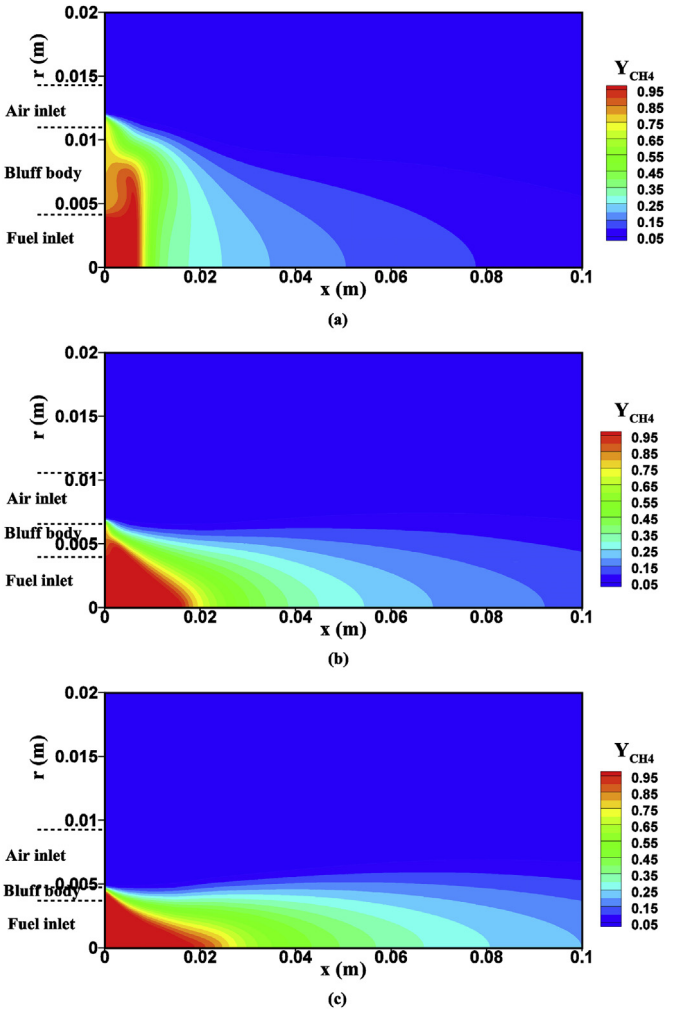

Fig. 14. The fuel mass fraction in a part of the combustion chamber, near the inlets, for a) $\xi = 0.5$, b) $\xi = 2$ (optimized case), and c) $\xi = 10$. The other parameters are $Q_f = 10$ lpm, $S = 0$, $A_a = 2$ cm^2, $\phi = 0.5$, $V_a = 15.876$ m/s, and $T_{inlet} = 298.15$ K.

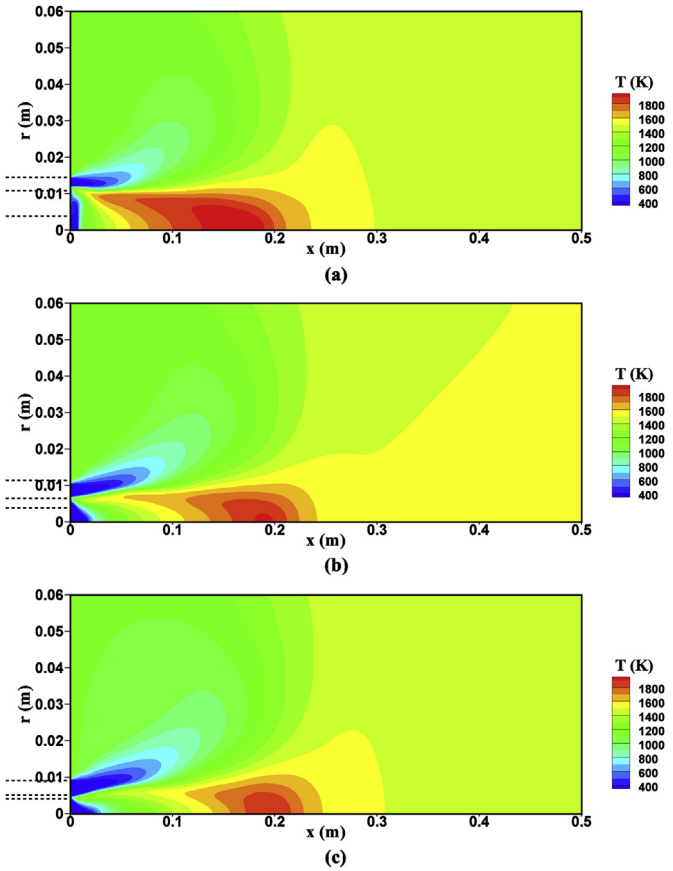

Fig. 15. The temperature distribution in the combustion chamber, for a) $\xi = 0.5$, b) $\xi = 2$ (optimized case), and c) $\xi = 10$. The other parameters are $Q_f = 10$ lpm, $S = 0$, $A_a = 2$ cm^2, $\phi = 0.5$, $V_a = 15.876$ m/s, and $T_{inlet} = 298.15$ K.

Next stage is to investigate the effect of swirling flow on the performance of the combustion chamber using EGM method. Both total entropy generation and maximum temperature within the combustion chamber for various swirl numbers are depicted in Fig. 17. As it can be seen in this figure, the total entropy generation increases very slightly by increasing the swirl number. In fact, by varying the swirl number in the range of 0–0.4, the total entropy generation changes by only 4% for $\xi = 2$ and $\phi = 0.5$. On the other hand, the maximum temperature increases by increasing the swirl number violating the MAT criterion. Therefore, the proposed value of the swirl number is $S = 0$ here. Note that, due to the limitation of our model, only the low to moderate swirl numbers are considered here which combine with the recirculating flow generated by the presence of the bluff. The variation of the entropy generation rate due to different phenomena by the change of the swirl number is also shown in Fig. 18. Increasing the swirl number causes the increase of the heat transfer entropy and decrease of chemical entropy generations. This variation is more tangible in the range $S < 0.2$ and after that it is not much recognizable.

The final step is to study the effect of air-inlet velocity on the performance of the combustion chamber. The total entropy generation for various air-inlet velocities is demonstrated in Fig. 19. As it is observed in this figure, the total entropy generation reduces slightly by decreasing the air-inlet velocity, V_a. By varying this parameter in the range of 3.969–31.752 m/s, the total entropy generation changes 6% for $\xi = 2$, $S = 0$ and $\phi = 0.5$. In addition, Fig. 19 shows that the maximum temperature in the chamber is approximately constant when V_a is larger than 15.876 m/s and increases sharply by decreasing its value beyond 15.876 m/s. Thus, in spite of the (slightly) smaller value of entropy generation for smaller air-inlet velocities, the optimum value of this parameter is $V_a = 15.876$ m/s to satisfy the MAT constraint. Fig. 20 shows the entropy generation rate due to each factor separately. It demonstrates that increasing the inlet air velocity causes the increase of the heat transfer entropy and decrease of chemical entropy

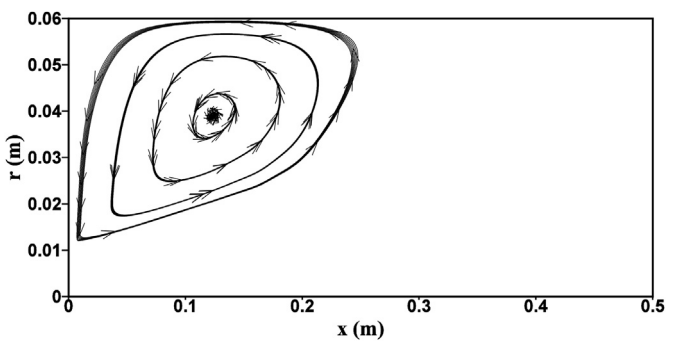

Fig. 16. Streamlines in the corner of the combustion chamber (corner recirculating region) corresponding to the case of Fig. 13(b).

Please cite this article in press as: Arjmandi HR, Amani E, A numerical investigation of the entropy generation in and thermodynamic optimization of a combustion chamber, Energy (2015), http://dx.doi.org/10.1016/j.energy.2014.12.077

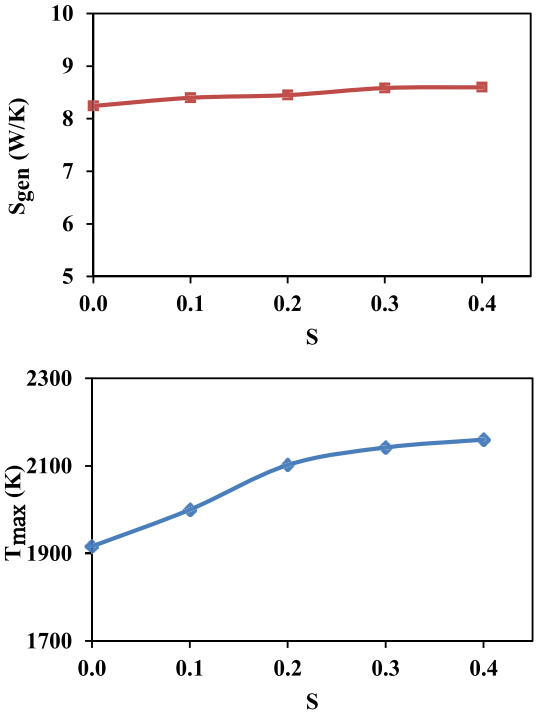

Fig. 17. The total entropy generation versus the swirl number computed using direct and indirect methods (up), and maximum temperature inside the combustion chamber versus the swirl number (down). The other parameters are $Q_f = 10$ lpm, $\xi = 2$, $A_a = 2$ cm^2, $\phi = 0.5$, $V_a = 15.876$ m/s, and $T_{inlet} = 298.15$ K.

generations. This change is sharper for cases with lower air-inlet velocities than 15 m/s and after that it is not much tangible.

4.3. The flame height as the second constraint

In practical design of energy systems, the geometrical constraints have to be considered almost always. One of the important factors which determine the size of a combustion chamber is the flame height because it is desirable that the combustion process develops completely before the flow leaves the combustion chamber, or the flame front is aimed to be far away from chamber's walls. Therefore, the increase of the flame height necessitates the use of larger chambers. For this reason, we consider the second constraint as the limiting value of the flame height.

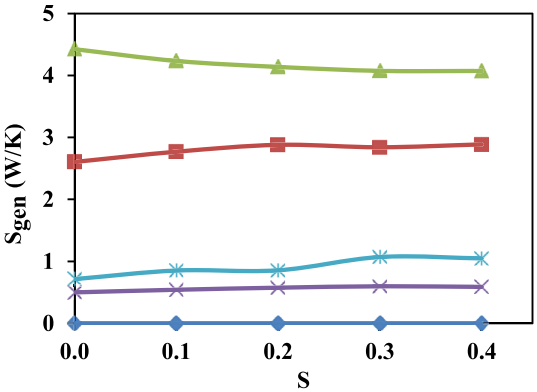

Fig. 18. The entropy generation rate due to different phenomena versus the swirl number. The other parameters are $Q_f = 10$ lpm, $\xi = 2$, $A_a = 2$ cm^2, $\phi = 0.5$, $V_a = 15.876$ m/s, and $T_{inlet} = 298.15$ K. Line legend: the same as Fig. 9.

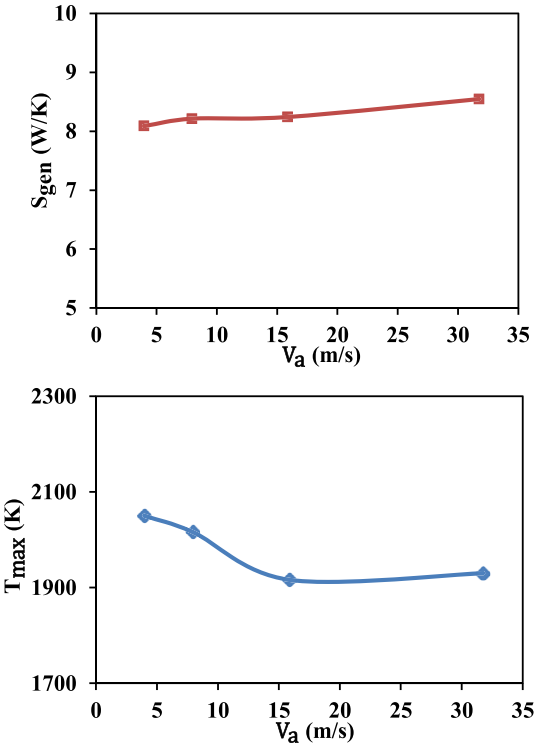

Fig. 19. The total entropy generation versus the air-inlet velocity using direct and indirect methods (up), and maximum temperature inside the combustion chamber versus the air-inlet velocity (down). The other parameters are $Q_f = 10$ lpm, $\xi = 2$, $A_a = 2$ cm^2, $S = 0$, $\phi = 0.5$, and $T_{inlet} = 298.15$ K.

Here, the flame height is calculated based on the mixture fraction definition with Bilger's coefficients as

$$Z = \frac{\frac{2}{M_C}(z_C - z_{C,2}) + \frac{1}{2M_H}(z_H - z_{H,2}) - \frac{1}{M_O}(z_O - z_{O,2})}{\frac{2}{M_C}(z_{C,1} - z_{C,2}) + \frac{1}{2M_H}(z_{H,1} - z_{H,2}) - \frac{1}{M_O}(z_{O,1} - z_{O,2})} \quad (28)$$

where z_i is the atomic mass fraction of atom i and the subscripts *1* and *2* refer to the value of z_i at the fuel- and air-inlet streams, respectively. The flame height is calculated as the maximum distance of the iso-value $Z = Z_{stoc} = 0.055$ from the center of the inlet-fuel nozzle.

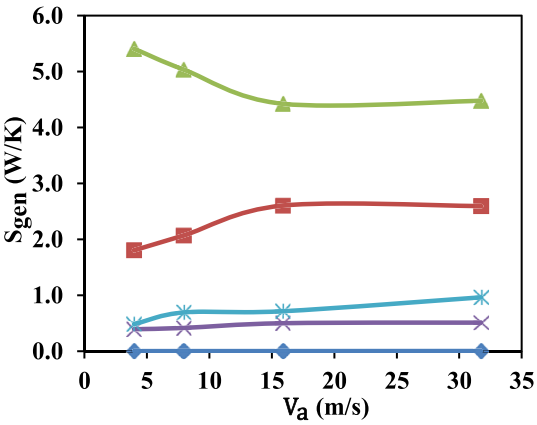

Fig. 20. The entropy generation rate due to different phenomena versus the air-inlet velocity. The other parameters are $Q_f = 10$ lpm, $\xi = 2$, $A_a = 2$ cm^2, $S = 0$, $\phi = 0.5$, and $T_{inlet} = 298.15$ K. Line legend: the same as Fig. 9.

Please cite this article in press as: Arjmandi HR, Amani E, A numerical investigation of the entropy generation in and thermodynamic optimization of a combustion chamber, Energy (2015), http://dx.doi.org/10.1016/j.energy.2014.12.077

The calculated flame height for all cases of Figs. 7, 11, 17 and 19 is reported in Fig. 21. As it is observed in this figure, the bluff-size has the weakest and the air-inlet velocity, especially for velocities smaller than 10 m/s, has the strongest effect on the variation of the flame height. Using the results reported in this figure, one can choose a limiting value for the flame height based on their specific size considerations. In our optimizations, we considered the value of 0.25 m as our second constraint. Therefore, the optimal design corresponds to the case with minimum entropy generation among all cases which satisfy the following two constraints.

$$\begin{aligned} &T_{max} \le \text{MAT} \approx 1900\ K \\ &\text{Flame height} \le 0.25\ m \end{aligned} \tag{29}$$

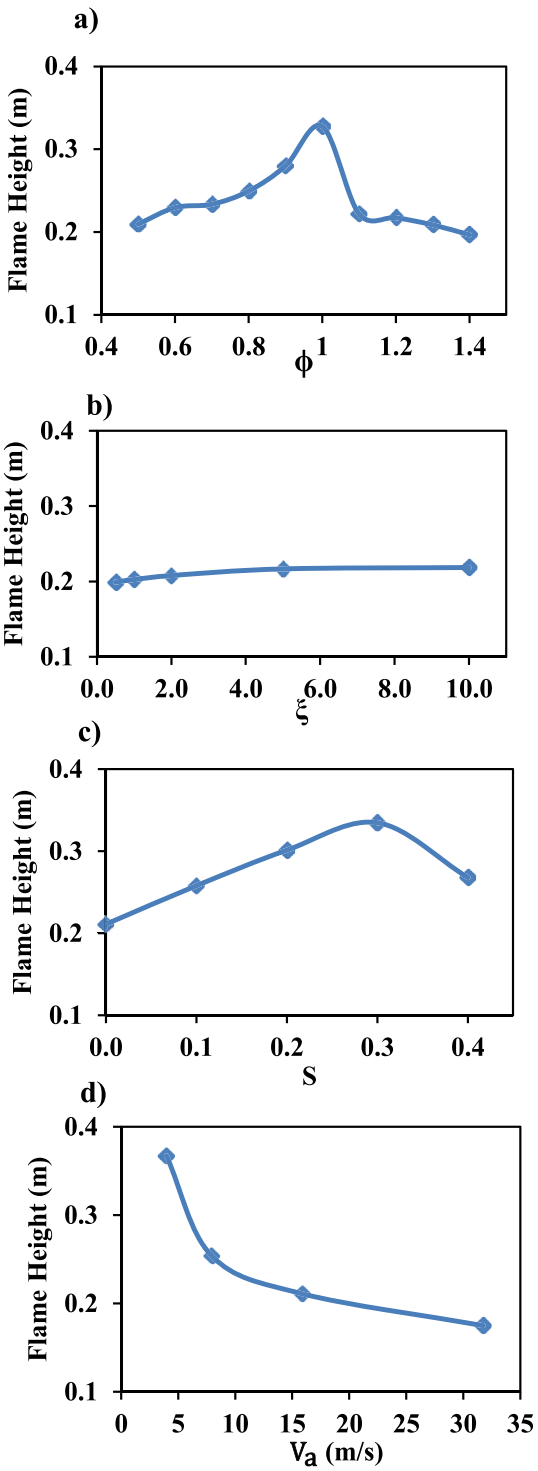

Fig. 21. The flame height for cases in a) Fig. 7 (Q_f = 10 lpm), b) Fig. 11, c) Fig. 17, and d) Fig. 19.

5. Conclusion

In this study, we simulate the turbulent combustion of a mixed bluff-body-swirl stabilized flame in a gas turbine combustion chamber. The governing equations are the continuity, momentum, species transport, and ideal gas law. The turbulence closure is provided by the RNG k-ε model in conjunction with the eddy-dissipation model for the averaged reaction rate. The governing equations are solved numerically using a finite volume method. Then, we use two methods, i.e. the direct and indirect methods, for calculating the entropy generation. After grid independency check and verifying our entropy generation computations by a simple analytical case, we investigate the effects of different parameters, including the equivalence ratio, fuel-inlet flow rate, bluff-size ratio, swirl number, and air-inlet velocity, on the entropy generation. We perform the design process of the combustion chamber by proposing the optimum value of each parameter based on the EGM method, i.e. by minimizing the total entropy generation under the two maximum allowable temperature and size constraints. We also conclude that the two direct and indirect methods, involving different approximations, differ by about 6% in average. The entropy generation rate due to chemical reaction composes the largest portion of the total entropy generation. The rates due to heat transfer, coupling between heat and mass transfer, mass transfer, and viscous friction have the next places, respectively. And finally, the entropy generations due to chemical reaction and heat transfer are opposing factors whose trade-off results in the optimum design condition.

Appendix A

The entropy generation rates, Eqs. (21a–e), in axisymmetric coordinates are written as

$$S'''_v = \frac{\mu_{\text{eff}}}{T}\left\{2\left[\left(\frac{\partial u_x}{\partial x}\right)^2 + \left(\frac{\partial u_r}{\partial r}\right)^2 + \left(\frac{u_r}{r}\right)^2\right] + \left(\frac{\partial u_x}{\partial r} + \frac{\partial u_r}{\partial x}\right)^2 + \left(\frac{\partial u_\theta}{\partial x}\right)^2 + \left(\frac{\partial u_\theta}{\partial r} - \frac{u_\theta}{r}\right)^2\right\} \tag{A-1a}$$

$$S'''_h = \frac{\lambda_{eff}}{T^2}\left[\left(\frac{\partial T}{\partial x}\right)^2 + \left(\frac{\partial T}{\partial r}\right)^2\right] \tag{A-1b}$$

$$S'''_m = \sum_i \frac{\rho \bar{R} D_{eff}}{Y_i M_i}\left[\left(\frac{\partial Y_i}{\partial x}\right)^2 + \left(\frac{\partial Y_i}{\partial r}\right)^2\right] \tag{A-1c}$$

$$S'''_{coupling} = \sum_i \frac{\rho s_i D_{eff}}{T}\left[\frac{\partial Y_i}{\partial x}\frac{\partial T}{\partial x} + \frac{\partial Y_i}{\partial r}\frac{\partial T}{\partial r}\right] \tag{A-1d}$$

$$S'''_{ch} = -\sum_i \frac{\mu_i \omega_i}{T} \tag{A-1e}$$

where, x, r, and θ are the axial, radial, and tangential directions, respectively. Note that u_θ is called swirl velocity.

Please cite this article in press as: Arjmandi HR, Amani E, A numerical investigation of the entropy generation in and thermodynamic optimization of a combustion chamber, Energy (2015), http://dx.doi.org/10.1016/j.energy.2014.12.077

References

[1] Bejan A. Entropy generation minimization. Boca Raton: CRC; 1996a.
[2] Bejan A. Entropy minimization: the new thermodynamics of finite-size devices and finite-time processes. J Appl Phys 1996b;79:1191–218.
[3] Li X, Faghri A. Local entropy generation analysis on passive high-concentration DMFCs (direct methanol fuel cell) with different cell structures. Energy 2011;36:403–14.
[4] Mahian O, Mahmud S, Heris S. Analysis of entropy generation between co-rotating cylinders using nanofluids. Energy 2012;44:438–46.
[5] Makhanlall D, Munda JL, Jiang P. Entropy generation in a solar collector filled with a radiative participating gas. Energy 2013;60:511–6.
[6] Escandón J, Bautista O, Méndez F. Entropy generation in purely electroosmotic flows of non-Newtonian fluids in a microchannel. Energy 2013;55:486–96.
[7] Ko TH, Ting K. Optimal Reynolds number for the fully developed laminar forced convection in a helical coiled tube. Energy 2006;31:2142–52.
[8] Ko TH. Thermodynamic analysis of optimal curvature for fully developed laminar forced convection in a helical coiled tube with uniform heat flux. Int J Therm Sci 2006;45:729–37.
[9] Jarungthammachote S. Entropy generation analysis for fully developed laminar convection in hexagonal duct subjected to constant heat flux. Energy 2010;35:5374–9.
[10] Amani E, Nobari MR. A numerical investigation of entropy generation in the entrance region of curved pipes at constant wall temperature. Energy 2011;36:4909–18.
[11] Amani E, Nobari MR. A numerical study of entropy generation in the entrance region of curved pipes. Heat Transf Eng 2010a;31(14):1203–12.
[12] Caton JA. A review of investigations using the second law of thermodynamics to study internal combustion engines. SAE paper no. 2000-01-1081. 2000.
[13] Caton JA. On the destruction of availability (exergy) due to combustion processes – with specific application to internal-combustion engines. Energy 2000b;25:1097–117.
[14] Rakopoulos CD, Kyritsis DC. Comparative second-law analysis of internal combustion engine operation for methane, methanol, and dodecane fuels. Energy 2001;26:705–22.
[15] Nakonieczny K. Entropy generation in a diesel engine turbocharging system. Energy 2002;27:1027–56.
[16] Rakopoulos CD, Kyritsis DC. Hydrogen enrichment effects on the second law analysis of natural and landfill gas combustion in engine cylinders. Int J Hydrogen Energy 2006;31:1384–93.
[17] Rakopoulos CD, Giakoumis EG. Second law analyses applied to internal combustion engines operation. Prog Energy Combust Sci 2006;32:2–47.
[18] Sieniutycz S. Analysis of power and entropy generation in a chemical engine. Int J Heat Mass Transf 2008;51:5859–71.
[19] Rakopoulos CD, Michos CN. Generation of combustion irreversibilities in a spark ignition engine under biogas–hydrogen mixtures fueling. Int J Hydrogen Energy 2009;34:4422–37.
[20] Knizley AA, Srinivasan KK, Krishnan SR, Ciatti SA. Fuel and diluent effects on entropy generation in a constant internal energy-volume (uv) combustion process. Energy 2012;43:315–28.
[21] Dash SK, Som SK. Transport processes and associated irreversibilities in droplet combustion in a convective medium. Int J Energy Res 1991;15:603–19.
[22] Datta A, Som SK. Thermodynamic irreversibilities and second law analysis in a spray combustion process. Combust Sci Technol 1999;142:29–54.
[23] Datta A. Entropy generation in a confined laminar diffusion flame. Combust Sci Technol 2000;159:39–56.
[24] Nishida K, Takagi T, Kinoshita S. Analysis of entropy generation and exergy loss during combustion. Proc Combust Inst 2002;29:869–74.
[25] Datta A. Effects of gravity on structure and entropy generation of confined laminar diffusion flames. Int J Therm Sci 2005;44:429–40.
[26] Stanciu D, Isvoranu D, Marinescu M. Second law analysis of diffusion flames. Int J Appl Thermodyn 2001;4:1–18.
[27] Yapıcı H, Gamze B, Kayata N, Albayrak B. Numerical study of effect of oxygen fraction on local entropy generation in a methane–air burner. Sadhana 2004;29:641–67.
[28] Yapıcı H, Gamze B, Kayata N, Albayrak B. Numerical calculation of local entropy generation in a methane–air burner. Energy Convers Manag 2005a;46:1885–919.
[29] Yapıcı H, Gamze B, Kayata N, Albayrak B. Effect of oxygen fraction on local entropy generation in a hydrogen–air burner. Heat Mass Transf 2006;43:37–53.
[30] Yapıcı H, Gamze B, Kayata N, Albayrak B. Numerical study on local entropy generation in a burner fueled with various fuels. Heat Mass Transf 2005b;41:519–34.
[31] Raghavan V, Gogos G, Babu V, Sundararajan T. Entropy generation during the quasi-steady burning of spherical fuel particles. Int J Therm Sci 2007;46:589–604.
[32] Stanciu D, Marinescu M, Dobrovicescu A. The influence of swirl angle on the irreversibilities in turbulent diffusion flames. Int J Thermodyn 2007;10:143–53.
[33] Som SK, Datta A. Thermodynamic irreversibilities and exergy balance in combustion processes. Prog Energy Combust Sci 2008;34:351–76.
[34] Briones AM, Mukhopadhyay A, Aggarwal SK. Analysis of entropy generation in hydrogen-enriched methane air propagating triple flames. Int J Hydrogen Energy 2009;34:1074–83.
[35] Chen S. Analysis of entropy generation in counter-flow premixed hydrogen air combustion. Int J Hydrogen Energy 2010;35:1401–11.
[36] Chen S, Li J, Han H, Liu Z, Zheng C. Effects of hydrogen addition on entropy generation in ultra-lean counter-flow methane-air premixed combustion. Int J Hydrogen Energy 2010c;35:3891–902.
[37] Chen S, Li J, Han H, Liu Z, Zheng C. Analysis of entropy generation in hydrogen-enriched ultra-lean counter-flow methane-air non-premixed combustion. Int J Hydrogen Energy 2010a;35:12491–501.
[38] Chen S, Li J, Han H, Liu Z, Zheng C. Analysis of entropy generation in non-premixed hydrogen versus heated air counter-flow combustion. Int J Hydrogen Energy 2010b;35:4736–46.
[39] Bidi M, Nobari MR, Avval MS. A numerical evaluation of combustion in porous media by EGM. Energy 2010;35:3483–500.
[40] Sheikhi MR, Safari M, Metghalchi H. Large eddy simulation for local entropy generation analysis of turbulent flows. J Energy Resour Technol 2012;134:1–6.
[41] Safari M, Sheikhi MR. Large eddy simulation for prediction of entropy generation in a nonpremixed turbulent jet flame. J Energy Resour Technol 2014;136:1–6.
[42] Emadi A, Emami MD. Analysis of entropy generation in a hydrogen-enriched turbulent non-premixed flame. Int J Hydrogen Energy 2013;38:5961–73.
[43] Makhanlall D, Munda JL, Jiang P. Radiation energy devaluation in diffusion combusting flows of natural gas. Energy 2013b;61:657–63.
[44] Farran R, Chakraborty N. A direct numerical simulation-based analysis of entropy generation in turbulent premixed flames. Entropy 2013;15:1540–66.
[45] Hosseini SE, Bagheri G, Wahid MA. Numerical investigation of biogas flameless combustion. Energy Convers Manag 2014;18:41–50.
[46] Jiang D, Yang W, Chua KJ, Ouyang J, Teng JH. Analysis of entropy generation distribution in micro-combustors with baffles. Int J Hydrogen Energy 2014;39:8118–25.
[47] Rana U, Chakraborty S, Som SK. Thermodynamics of premixed combustion in a heat recirculating micro combustor. Energy 2014;68:510–8.
[48] Gicquel LY, Staffelbach G, Poinsot T. Large Eddy simulations of gaseous flames in gas turbine combustion chambers. Prog Energy Combust Sci 2012;38:782–817.
[49] Westbrook CK, Dryer FL. Simplified reaction mechanisms for the oxidation of hydrocarbon fuels in flames. Combust Sci Technol 1981;27:31–43.
[50] Burcat's A. (n.d.). Retrieved 11 11, 2014, from: garfield.chem.elte.hu/Burcat/THERM.DAT.
[51] Rosner DE. Transport processes in chemically reacting flow system. London: Butterworths; 1986.
[52] Teng H, Kinoshita CM, Masutani SM, Zhou J. Entropy generation in multi-component reacting flows. J Energy Resour Technol 1998;120:226–32.
[53] Morinishi Y. Skew-symmetric form of convective terms and fully conservative finite difference schemes for variable density low-Mach number flows. J Comput Phys 2010;229:276–300.
[54] Patankar SV. Numerical heat transfer and fluid flow. New York: McGraw Hill; 1983.
[55] Barth TJ, Jespersen D. The design and application of upwind schemes on unstructured meshes. Technical Report AIAA-89–0366. In: AIAA 27th Aerospace Sciences Meeting, Reno, Nevada; 1989.
[56] Barlow, R., & Frank, J. (n.d.). Retrieved 10 3, 2014, from: http://www.sandia.gov/TNF/DataArch/FlameD.html.
[57] Amani E, Nobari MR. An efficient PDF calculation of flame temperature and major species in turbulent non-premixed flames. Appl Math Model 2010b;34:2223–41.
[58] Xu X, Chen Y, Wang H. Detailed numerical simulation of thermal radiation influence in Sandia Flame D. Int J Heat Mass Transf 2006;49:2347–55.

Please cite this article in press as: Arjmandi HR, Amani E, A numerical investigation of the entropy generation in and thermodynamic optimization of a combustion chamber, Energy (2015), http://dx.doi.org/10.1016/j.energy.2014.12.077